

DMD # 73890

Application of static modeling in the prediction of *in vivo* drug-drug interactions between rivaroxaban and anti- arrhythmic agents based on *in vitro* inhibition studies

Eleanor Jing Yi Cheong, Janice Jia Ni Goh, Yanjun Hong, Gopalakrishnan Venkatesan, Yuanjie Liu,
Gigi Ngar Chee Chiu, Pipin Kojodjojo and Eric Chun Yong Chan

Department of Pharmacy, Faculty of Science, National University of Singapore, 18 Science Drive 4,
Singapore 117543 (E.J.Y.C, J.J.N.G, Y.H, G.V, Y.L, G.N.C.C, E.C.Y.C); Department of Chemistry,
Faculty of Science, Hong Kong Baptist University, Cha Chi-ming Science Tower, Ho Sin Hang
Campus, Hong Kong (Y.H); Department of Cardiology and Cardiac Electrophysiology, National
University Heart Centre, 5 Lower Kent Ridge Road, Singapore 119074 (P.K); Singapore Institute for
Clinical Sciences (SICS), Brenner Centre for Molecular Medicine, 30 Medical Drive, Singapore
117609 (E.C.Y.C)

DMD # 73890

Running title: Interactions between rivaroxaban and anti-arrhythmic agents

Address correspondence to:

Associate Professor Eric Chun Yong Chan, Department of Pharmacy, Faculty of Science, National University of Singapore, Block S7, Level 2, 18 Science Drive 4, Singapore 117543, Singapore.

Email: phaccye@nus.edu.sg; Telephone: 65-6516 6137; Fax: +65-67791554

Number of Text Pages	16
Number of Tables	5
Number of Figures	6
Number of References	35
Number of Words in the Abstract	246
Number of Words in the Introduction	661
Number of Words in the Discussion	1500

ABBREVIATIONS

ACN	Acetonitrile
AF	Atrial Fibrillation
CYP2J2	Cytochrome P450 2J2
CYP3A4	Cytochrome P450 3A4
CYP3A5	Cytochrome P450 3A5
DDI	Drug-drug interaction
FDA	United States Food and Drug Administration
f_m	Fraction of the total clearance to which the affected P450 enzyme contributes
F_G	Fraction of the dose of the affected drug that passes through the intestine unchanged after p.o. administration

DMD # 73890

$[I]_H, [I]_G$	Concentration of inactivator at the active site in the liver and the gut respectively
k_{deg}	First order rate constant of <i>in vivo</i> degradation of the CYP enzymes
K_i	Reversible inhibition constant
K_I	Inactivator concentration at half-maximum inactivation rate constant
k_{inact}	Maximum inactivation rate constant
K_m	Michaelis-Menten constant
k_{obs}	Observed rate of inactivation
LC/MS/MS	Liquid chromatography in tandem with mass spectrometry
MBI	Mechanism-based inactivation
MRM	Multiple Reaction Monitoring
NDBD	<i>N</i> -desbutyldronedarone
NDEA	<i>N</i> -desethylamiodarone
P-gp	P-glycoprotein
rCYP2J2	Recombinant Cytochrome P450 2J2
rCYP3A4	Recombinant Cytochrome P450 3A4
V_{max}	Maximum rate of reaction

DMD # 73890

ABSTRACT

Rivaroxaban, a direct Factor Xa inhibitor, is indicated for stroke prevention in non-valvular atrial fibrillation (AF). Studies have revealed that the clearance of rivaroxaban is largely attributed to CYP3A4, CYP2J2 metabolism and P-gp efflux pathways. Amiodarone and dronedarone are anti-arrhythmic agents employed in AF management. Amiodarone, dronedarone and their major metabolites, *N*-desethylamiodarone (NDEA) and *N*-desbutyldronedarone (NDBD) demonstrate inhibitory effects on CYP3A4 and CYP2J2 with FDA recommended probe substrates. Additionally, both amiodarone and dronedarone are known P-gp inhibitors. Hence, the concomitant administration of these anti-arrhythmic agents has the potential to augment the systemic exposure of rivaroxaban through simultaneous impairment of its clearance pathways. Currently, however, there is a lack of clinical data on the extent of these postulated DDIs. In this study, *in vitro* inhibition assays using rivaroxaban as the probe substrate demonstrated that both dronedarone and NDBD produced reversible inhibition as well as irreversible mechanism-based inactivation (MBI) of CYP3A4- and CYP2J2-mediated metabolism of rivaroxaban. However, amiodarone and NDEA were observed to cause reversible inhibition as well as MBI of CYP3A4 but not CYP2J2. Additionally, amiodarone, NDEA and dronedarone but not NDBD were determined to inhibit P-gp mediated rivaroxaban transport. The *in vitro* inhibition parameters were fitted into a mechanistic static model which predicted a 37% and 31% increase in rivaroxaban exposure due to the inhibition of hepatic and gut metabolism by amiodarone and dronedarone respectively. A separate model quantifying the inhibition of P-gp mediated efflux by amiodarone or dronedarone projected a 9% increase in rivaroxaban exposure.

DMD # 73890

Chemical compounds cited in this article

Amiodarone hydrochloride (PubChem CID: 441325); Dronedarone hydrochloride (PubChem CID: 219025); Dronedarone (PubChem CID: 208898); *N*-desethylamiodarone (PubChem CID: 104774); *N*-desbutyldronedarone (PubChem CID: 10255437); Rivaroxaban (PubChem CID: 9875401); Amprenavir (PubChem CID: 65016); Propranolol (PubChem CID: 4946)

DMD # 73890

INTRODUCTION

Atrial fibrillation (AF) is the most commonly sustained and clinically significant cardiac arrhythmia affecting approximately 33.5 million people worldwide in 2010 (Chugh *et al.*, 2014). As the prevalence of AF increases with age, the global burden of the disease is projected to increase exponentially, creating a significant public health burden (Rahman *et al.*, 2014). Therapeutic cornerstones of AF management include ventricular rate control, maintenance of sinus rhythm using antiarrhythmic therapy and prevention of stroke and systemic embolism using anticoagulants (January *et al.*, 2014).

Rivaroxaban (Xarelto, Janssen Pharmaceuticals, Inc., Beerse Belgium), an inhibitor of Factor Xa of the coagulation cascade, was approved in 2011 as a novel non-Vitamin K oral anticoagulant. It is indicated for the reduction of risk of stroke and systemic embolism in patients with non-valvular AF (US FDA, 2011b). Studies have revealed that approximately two thirds of the administered rivaroxaban dose undergoes metabolic clearance in the liver, with contributions from cytochrome P450 (CYP) enzymes, namely CYP3A4, CYP2J2 and hydrolytic enzymes (Weinz *et al.*, 2009). The remaining one third of the given dose is eliminated in the urine largely via P-glycoprotein (P-gp) and breast cancer resistance protein (BCRP [ABCG2]) mediated secretion (Gnoth *et al.*, 2011). A previous physiologically-based pharmacokinetic (PBPK) modeling study characterized a drug-drug-disease interaction, where the synergistic combination of renal impairment coupled with moderate CYP3A4 inhibition culminated in a clinically significant increase in rivaroxaban exposure (Grillo *et al.*, 2012). Outcomes of this simulation eventually led to recommendations cautioning against the concomitant administration of moderate CYP3A4/P-gp inhibitors with rivaroxaban in the presence of any degree of renal impairment (US FDA, 2011b). This attests to the inherent susceptibility of rivaroxaban to complex drug-drug interactions (DDIs) mediated through simultaneous impairment of its multiple clearance pathways. Given its steep exposure-major bleeding relationship (US FDA, 2011a), it is thus imperative to identify clinical relevant DDI scenarios that could augment rivaroxaban exposure.

DMD # 73890

A subgroup analysis of the ROCKET AF trial studying the efficacy and safety of rivaroxaban highlighted the potential combination of antiarrhythmic drug therapy and anticoagulation as mainstays in AF management and concluded that the concomitant use of amiodarone and rivaroxaban warrants further investigation (Steinberg *et al.*, 2014). Dronedarone (Multaq, Sanofi Aventis, Bridgewater, NJ) was approved in 2009 as a structural analogue of amiodarone (US FDA, 2009a). In a bid to minimize the extracardiac adverse effects associated with amiodarone, iodine substituents were eliminated to avoid amiodarone-linked thyroid toxicities and a methane-sulfonamide group was added to reduce tissue accumulation (**Fig. 1A and 1B**) (US FDA, 2009).

Both amiodarone (**Fig. 1A**) and dronedarone (**Fig. 1B**) undergo extensive metabolism by CYP3A4/3A5 to form pharmacologically active metabolites *N*-desethylamiodarone (NDEA) (**Fig. 1C**) and *N*-desbutyldronedarone (NDBD) (**Fig. 1D**) respectively (Fabre *et al.*, 1993; Klieber *et al.*, 2014). Additionally, both drugs are substrates of CYP2J2 (Lee *et al.*, 2010; Karkhanis *et al.*, 2016). The common structural features in these antiarrhythmic agents and their metabolites are the alkylamine and furan that are in turn associated with mechanism-based inactivation (MBI) of CYP450 (Orr *et al.*, 2012). Indeed, corroborating previous findings, our laboratory established the reversible and irreversible inhibition of CYP3A4- and CYP2J2-mediated metabolism of US FDA recommended probe substrates by amiodarone and NDEA (Ohyama *et al.*, 2001; McDonald *et al.*, 2015; Karkhanis *et al.*, 2016) as well as dronedarone and NDBD (Hong *et al.*, 2015; Karkhanis *et al.*, 2016). Independently, amiodarone and dronedarone have been reported as P-gp inhibitors (US FDA, 2009b, 2012).

Taken together, we hypothesized that amiodarone, dronedarone, NDEA and NDBD could increase systemic exposure of rivaroxaban via their inhibitory effects on CYP3A4, CYP2J2 and P-gp. To date, there remains a paucity of clinical data on the DDIs between rivaroxaban and these antiarrhythmic agents. This study aimed to quantitatively predict the *in vivo* DDI risk between rivaroxaban and amiodarone or dronedarone via mechanistic static modeling. In order to characterize the multi-faceted DDIs and generate the inhibitory parameters accurately, rivaroxaban was utilized as the probe

DMD # 73890

substrate in place of the respective US FDA recommended probe substrates of CYP3A4, CYP2J2 and P-gp.

DMD # 73890

MATERIALS AND METHODS

In this study, *in vitro* inhibition data encompassing reversible inhibition, MBI and inhibition of P-gp mediated efflux were fitted into mechanistic static models that provided the framework for quantitative predictions of either metabolic or transporter based DDIs between rivaroxaban and the antiarrhythmic drugs.

Chemicals. High performance liquid chromatography-grade acetonitrile (ACN) was purchased from Tedia Company Inc. (Fairfield, OH). Amiodarone hydrochloride, dronedarone hydrochloride, NDBD, NDEA, rivaroxaban and verapamil hydrochloride were acquired from Sigma-Aldrich (St. Louis, MO). Amprenavir was purchased from Toronto Research Chemicals Inc. (Toronto, ON, Canada). Human recombinant cytochrome P450 supersomes (rCYP) and NADPH regenerating system consisting of NADPH A (NADP⁺ and glucose-6-phosphate) and B (glucose-6-phosphate dehydrogenase) were obtained from BD Gentest (Woburn, MA). Water was obtained using a milli-Q water purification system (Millipore, Billerica, MA). For cell culture, Dulbecco's modified eagle's medium (DMEM) with phenol red, Dulbecco's phosphate buffer solution (DBPS), foetal bovine serum (FBS) and 10,000 IU antibiotic solution (penicillin/streptomycin) were obtained from Gibco Life Technologies (Waltham, MA, USA). Lucifer yellow CH dilithium salt was from Invitrogen Corporation (Carlsbad, CA, USA). L-glutamine was from Hyclone Laboratories (Logan, UT, USA). Sodium bicarbonate powder was from Sigma Aldrich (St. Louis, MO, USA). All other reagents were of analytical grade.

Reversible Inhibition of CYP3A4 and CYP2J2 by amiodarone, dronedarone and their metabolites. Amiodarone, dronedarone and their metabolites (i.e. NDEA and NDBD) were tested as reversible inhibitors using rivaroxaban as the probe substrate. Experiments were performed in 96-well plates and all samples were carried out in triplicates. Rivaroxaban (2.5, 5, 15, 30 and 50 μ M) was pre-incubated at 37°C for 5 min with 20 pmol/mL recombinant CYP enzymes, NADPH B and 100 mM potassium phosphate buffer (pH 7.4) across 7 concentration levels of the inhibitors (amiodarone: 0-5 μ M; dronedarone, NDEA and NDBD: 0-10 μ M). The reactions were initiated by the addition of 5 μ L NADPH A, yielding a final incubation mixture of 100 μ L with 1% ACN (v/v). Incubation was carried

DMD # 73890

out at 37°C for either 2 h with CYP3A4 or 30 min with CYP2J2 before an 80 μ L aliquot was removed and quenched with an equal volume of ice-cold ACN containing 0.005 μ M verapamil (internal standard). The quenched samples were subjected to centrifugation at 2755 g, 4°C for 30 min. Subsequently, the supernatants were removed for the determination of morpholinone hydroxylated metabolite (main metabolite) of rivaroxaban by LC/MS/MS analysis (**Supplemental Methods and Supplemental Table 1**). The data were first fitted to the Michaelis-Menten model. Subsequently, Lineweaver Burk plots were applied to predict the mode of reversible inhibition. The apparent equilibrium dissociation constant (K_i) for the enzyme-inhibitor complex was determined by non-linear least squares regression based on the best model of reversible inhibition.

Time- and concentration-dependent inactivation of CYP3A4 and CYP2J2 by amiodarone, dronedarone and their metabolites. Rivaroxaban was used as the probe substrate in this experiment. Incubations (n=3) were conducted in 96-well plates. Primary incubation mixtures comprising various concentration levels of amiodarone (0-5 μ M) or NDEA (0-1 μ M) were pre-incubated at 37°C for 5 min with recombinant CYP enzymes (20 pmol/mL) and NADPH B in potassium phosphate buffer (100 mM, pH 7.4). To initiate the enzymatic reaction, 5 μ L of NADPH A was added to the primary incubation. The final primary incubation mixture volume was 100 μ L and contained <1% v/v organic solvent. At different pre-incubation time points (0, 3, 8, 15, 22, 30, 45 min) after the addition of NADPH A, 5 μ L aliquots of the primary incubation was transferred to 95 μ L of the secondary incubation containing 50 μ M rivaroxaban, the NADPH regenerating system and 100 mM potassium phosphate buffer (pH 7.4) to yield a 20-fold dilution. The secondary incubation mixtures were incubated at 37°C for 2 h with CYP3A4 or 30 min with CYP2J2 before 80 μ L aliquots were removed and quenched with an equal volume of ice-cold ACN containing 0.005 μ M verapamil (internal standard). The same morpholinone hydroxylated metabolite was quantified using LC/MS/MS (**Supplemental Methods and Supplemental Table 1**). Inactivation of CYP3A4 (40 pmol/mL) and CYP2J2 (20 pmol/mL) by dronedarone (0-2.5 μ M) and NDBD (0-5 μ M) was investigated using the same two step incubation protocol except with a 10-fold dilution into the secondary incubation.

DMD # 73890

Calculation of Inactivation Kinetic Parameters (K_I and k_{inact}). The mean of triplicate peak area ratios was normalized to 0 min with respect to pre-incubation time. The percentage probe substrate activity remaining was computed and the natural logarithmic activity plotted against inactivation pre-incubation time for each inactivator concentration. The data were fitted to linear regression and k_{obs} values (apparent inactivation rate constants) were calculated as the negative slopes of the lines. Subsequently, a plot of k_{obs} values against inactivator concentration [I] allowed the fitting of inactivation kinetic parameters (K_I and k_{inact}) to non-linear least squares regression based on **Equation 1** in GraphPad PRISM[®] software version 6.01 (San Diego, CA, USA).

$$k_{obs} = \frac{k_{inact} \times [I]}{K_I + [I]} \quad (1)$$

In Equation 1, k_{inact} represents the maximum inactivation rate constant at infinite inactivator concentration; K_I is the concentration of inactivator at the half-maximum rate of inactivation and [I] is the *in vitro* inactivator concentration.

Inhibition of P-gp efflux of rivaroxaban by amiodarone, dronedarone and their metabolites.

Madin-Darby canine kidney sub-clone I cells transfected with multi drug resistance protein 1 (MDCK-MDR1) were maintained in DMEM culture media supplemented with 10% FBS, L-glutamine (862 mg/L) and 1% penicillin/streptomycin. For transport studies, cells were first seeded at a density of 250,000 cells/well and culture media was refreshed after 24 h. At approximately 48 h post-seeding, culture media was first removed and each well and insert were rinsed gently with PBS to ensure no residual metabolic waste. Test inhibitors were dissolved in methanol whereas rivaroxaban was reconstituted in ACN and dimethyl sulfoxide (DMSO) at lower (2 mM) and higher concentration (20 mM) levels respectively. Dilutions for all compounds were carried out using ACN. Triplicate sets of wells were used to assess the apparent permeability of rivaroxaban from the apical (A) to basolateral (B) chambers [P_{app} (A→B)] and B to A [P_{app} (B→A)]. To initiate transport, the donor solution was first added followed by the receiver solution. All experiments were carried out at room temperature ($24 \pm 1^\circ\text{C}$). Amprenavir (10 μM) and propranolol (25 μM) were used as positive

DMD # 73890

controls (substrate and inhibitor respectively). P_{app} (A→B) of lucifer yellow (100 μ M) was utilized as a marker of monolayer integrity. The fluorescence of lucifer yellow of each apical and basolateral solution was measured at an excitation wavelength of 430 nm and emission wavelength of 540 nm using a Tecan Infinite® F500 plate reader (Männedorf, Switzerland). Acceptance criterion for a confluent monolayer was defined as lucifer yellow permeability of less than 80 nm/s.

To ensure P-gp assay sensitivity, experiments were first performed to investigate the potential for both concentration and time-dependent saturation of the transport of rivaroxaban via P-gp (**Supplemental Methods**). The optimal incubation time was eventually determined to be 90 min and a rivaroxaban concentration of 10 μ M was also selected (**Supplemental Fig. 1 and 2**). Subsequently, 25 and 12.5 μ M of each inhibitor (i.e. amiodarone, dronedarone, NDEA and NDBD) were first subjected to a preliminary study to estimate their IC_{50} values. The inhibitor concentrations were subsequently optimized to encompass the IC_{50} and ensure inhibition assay sensitivity. The receiver solution was collected and stored at -20°C for further sample processing prior to LC/MS/MS analysis (**Supplemental Methods**). In order to determine the mode of P-gp inhibition, 3 inhibitor concentration levels in proximity of the IC_{50} value were assayed against 2 concentration levels of rivaroxaban (5 and 20 μ M). A Dixon plot was generated to predict the mode of P-gp inhibition as well as determine the K_i values.

Estimating the extent of metabolic DDI using a mechanistic static model. The kinetic constants accounting for reversible inhibition (i.e. K_i) and time-dependent inactivation (i.e. k_{inact} , K_I) of the drug metabolizing enzymes were incorporated into a mechanistic static model developed previously by Fahmi *et al* (Fahmi *et al.*, 2008) and refined by Isoherranen *et al* (Isoherranen *et al.*, 2012) to account for multi P450 inhibition. The proposed model accounts for the contributions of enzyme inhibition both in the liver and within the gut wall in predicting the extent of DDI. The area under the curve ratio (AUCR) in the presence of a pharmacokinetic DDI is described by **Equation 2**.

$$AUCR = \frac{1}{\sum_i^n [f_{m,P450i} \times (A \times B)] + (1 - \sum_i^n f_{m,P450i})} \times \frac{1}{[X \times Y] \times (1 - F_G) + F_G} \quad (2)$$

DMD # 73890

The terms are defined as follows:

A is the term for time-dependent inactivation observed in the liver for each of the P450 enzymes inactivated,

$$A = \frac{k_{deg,H}}{k_{deg,H} + \frac{[I]_H \times k_{inact}}{[I]_H + K_i}}$$

B is the term for reversible inhibition in the liver for each of the P450 enzymes inactivated,

$$B = \frac{1}{1 + \frac{[I]_H}{K_i}}$$

X is the term for time-dependent inactivation of CYP3A4 observed in the intestine,

$$X = \frac{k_{deg,G}}{k_{deg,G} + \frac{[I]_G \times k_{inact}}{[I]_G + K_i}}$$

Y is the term for reversible inhibition of CYP3A4 in the intestine,

$$Y = \frac{1}{1 + \frac{[I]_G}{K_i}}$$

where $[I]_H$ and $[I]_G$ represent *in vivo* concentrations of the inhibitor available to the enzyme in the liver and intestine respectively (**Table 1**). The degradation rates for CYP3A4 in the liver ($k_{deg,H}$) and intestine ($k_{deg,G}$) were 0.00032 and 0.00048 min^{-1} based on $t_{1/2}$ of 36 h and 24 h (Fahmi *et al.*, 2008). For CYP2J2, there is insufficient clinical pharmacokinetic data to perform similar calculations. As a result, the average of the calculated estimates for the various hepatic CYP enzymes (0.00026 min^{-1}) was used (Yang *et al.*, 2008). The fraction of rivaroxaban metabolized by CYP3A4 ($f_{m,CYP3A4}$) and CYP2J2 ($f_{m,CYP2J2}$) has been reported to be 0.18 and 0.14 respectively (Mueck *et al.*, 2014) whereas the fraction of rivaroxaban escaping intestinal extraction (F_G) was calculated to be 0.89 (see **Supplemental Methods**).

Estimating the extent of transporter mediated DDI using a mechanistic static model. The kinetic constant describing the inhibition of P-gp mediated efflux of rivaroxaban was fitted into another mechanistic static model developed to examine the effect of inhibition of renal secretion transporters

DMD # 73890

on plasma exposure of the victim drug (Feng *et al.*, 2013). The AUC ratio of the victim drug in the presence and absence of the inhibitor is summarized in **Equation 3**.

$$AUCR = \frac{1 + \frac{CL_{sec,c}}{CL_x}}{1 + \frac{CL_{sec,c}}{CL_x} \cdot \frac{1}{1 + \left(\frac{[I]}{K_i}\right)}} = \frac{1}{1 - \frac{CL_{sec,c}}{CL} \cdot \frac{\left(\frac{[I]}{K_i}\right)}{1 + \frac{[I]}{K_i}}} \quad (3)$$

where [I] represents the maximum plasma concentration of the inhibitor (**Table 1**). The net secretory clearance of rivaroxaban ($CL_{sec,c}$) (55.6 mL/min) was approximated to be five sixth of total plasma renal clearance (66.7 mL/min) (Mueck *et al.*, 2014). The total plasma clearance (CL) of rivaroxaban has been reported to be 166.7 mL/min and is a composite of the hepatic and renal clearances (Mueck *et al.*, 2014).

RESULTS

Reversible Inhibition of CYP3A4 and CYP2J2 by amiodarone, dronedarone and their metabolites. The reversible inhibition of CYP3A4 and CYP2J2 by amiodarone, dronedarone and their metabolites was investigated using the peak area of rivaroxaban metabolite as a proxy for the rate of product formation. Rivaroxaban was evaluated across 5 concentration levels spanning its K_m in the presence of varying concentrations of amiodarone, dronedarone, NDEA and NDBD. In a preliminary study of reversible inhibition of CYP2J2 by amiodarone and NDEA, high concentrations of both amiodarone and NDEA were easily overcome by a small increase in rivaroxaban concentration, thus suggesting that amiodarone and NDEA did not inhibit CYP2J2 with rivaroxaban as the probe substrate (**Supplemental Fig. 3A**). However, based on the inhibition kinetics plots (**Fig. 2A-B**) and their respective Lineweaver Burk plots (**Fig. 2C-D**), dronedarone and NDBD were established to be mixed competitive inhibitors of CYP2J2 when rivaroxaban was used as the probe substrate. On the other hand, amiodarone and NDEA exhibited mixed competitive inhibition of CYP3A4 (**Fig. 3A-B and 3E-F**) whereas dronedarone and NDBD demonstrated competitive inhibition (**Fig. 3C-D and 3G-H**). The calculated inhibition constants K_i of the relevant inhibitors against the respective enzymes are presented in **Table 2**.

Time- and concentration-dependent inactivation of CYP3A4 and CYP2J2 by amiodarone, dronedarone and their metabolites. To investigate the MBI of CYP3A4 and CYP2J2 by amiodarone, dronedarone and their metabolites, rivaroxaban was used as the probe substrate and the rate of hydroxylation at the morpholinone moiety of rivaroxaban was monitored and used as a surrogate for enzymatic activity. In the presence of NADPH, a time-dependent decrease in CYP2J2 enzymatic activity was not observed when pre-incubated with amiodarone (5 μ M and 50 μ M) and NDEA (**Supplemental Fig. 3B and 3C**). However, time-dependent inactivation of CYP2J2 was demonstrated in the presence of dronedarone and NDBD. Pre-incubation of CYP2J2 with increasing concentration levels of either dronedarone or NDBD resulted in concentration-dependent increased

DMD # 73890

rate of inactivation of enzymatic activity. The observed first order rates of inactivation (k_{obs}) calculated from various concentrations of dronedarone (**Fig. 4A**) and NDBD (**Fig. 4B**) followed saturation kinetics that approached a maximum rate of inactivation (**Fig. 4C-D**). Likewise, as presented in **Fig. 5A-D**, time- and concentration-dependent inactivation of CYP3A4 were established for both amiodarone, dronedarone and their metabolites. Kinetic plots (k_{obs} versus inactivator concentration) also demonstrated saturation kinetics (**Fig. 5E-H**). Calculated inactivation kinetic parameters, K_I and k_{inact} , are summarized in **Table 3**. The efficiency of enzyme inactivation (k_{inact}/K_I ratio) is also reported.

Cell Monolayer Integrity and Compound Recovery. A-to-B flux determinations of lucifer yellow were used to confirm monolayer integrity when co-incubated with the highest concentration levels of the test substrate and inhibitors. This data confirmed that the monolayer was intact under these extreme conditions and validated its suitability for subsequent permeability studies. Using LLE, high recovery of rivaroxaban ~ 100 % and accurate linear calibration (+/- 20 % accuracy and r^2 0.99) were achieved reproducibly from 0.01-10 μ M. For rivaroxaban concentrations above 10 μ M, saturation of the detector was observed and the samples were diluted using DMEM before sample processing in order to ensure its accurate quantitation. Percentage recovery of rivaroxaban from the apical and basolateral chambers at the end of the assay (mass balance) was greater than 80%, indicating that no significant amount of rivaroxaban was lost during sample transfer and processing nor in MDCK-MDR1, hence demonstrating the reliability of measured P_{app} values.

P-gp inhibitory IC_{50} and K_i of test inhibitors. The concentration-dependent inhibitory effect of amiodarone, dronedarone and their metabolites on transport of rivaroxaban across MDCKII monolayers was tested. IC_{50} is the inhibitor concentration needed to decrease the efflux ratio by half. Amiodarone (**Fig. 6A**) and NDEA (**Fig. 6B**) yielded similar IC_{50} values of 10.3 μ M and 9.20 μ M respectively. Based on an IC_{50} of 1.83 μ M (**Fig. 6C**), dronedarone was determined to be the most potent P-gp inhibitor while NDBD demonstrated little P-gp inhibition activity as seen from its high IC_{50} value of 76.3 μ M (**Fig. 6D**). Subsequently, the respective inhibitory concentrations that produced

DMD # 73890

a linear decrease in efflux ratio were chosen for the Dixon plots (data not shown) where we confirmed amiodarone's noncompetitive allosteric inhibition of Pgp efflux of rivaroxaban (5 and 20 μM) with K_i at 8.94 μM while dronedarone demonstrated competitive inhibition with K_i at 0.68 μM . Assuming the same mode of non-competitive inhibition of P-gp, the K_i value of NDEA was determined to be 5.36 μM . The K_i value of NDBD was not further elucidated as its high IC_{50} value was predicted not to produce meaningful inhibitory potential.

Static modeling of metabolic and transport based DDIs. *In vitro* inactivation (k_{inact} and K_I) and inhibition (K_i) parameters were subsequently incorporated into a mechanistic static model (**Equation 2**) that permits comprehensive evaluation of the potential impact of MBI and reversible inhibition of CYP3A4 and CYP2J2 on the systemic exposure of rivaroxaban. In the assessment of metabolic DDI potential using AUC fold change, inhibition of hepatic metabolism of rivaroxaban by amiodarone, NDEA, dronedarone and NDBD was predicted to produce AUC fold changes of 1.22, 1.22, 1.17 and 1.26 respectively (**Table 4**). When the combined effects of altered hepatic and intestinal metabolism were considered, there was an increase in the AUC fold change precipitated by amiodarone and dronedarone to 1.37 and 1.31 (**Table 4**). Transporter mediated DDI was quantitatively determined by fitting *in vitro* parameters describing inhibition of P-gp mediated efflux of rivaroxaban into **Equation 3**. As summarized in **Table 4**, the eventual AUC fold change was 1.09 for both dronedarone and amiodarone whereas NDEA produced a slightly higher AUC fold change of 1.13.

DISCUSSION

The application of *in vitro* methodologies to evaluate the inhibitory potential of a drug entity and assess the likelihood of *in vivo* drug interactions is a critical aspect of the drug development and regulatory review paradigm (Zhang *et al.*, 2009). In this study, we quantified the *in vitro* inhibition parameters to characterize the DDI between rivaroxaban and the antiarrhythmic agents.

Rivaroxaban was not tested as a substrate in previous in house studies investigating the CYP3A4 and CYP2J2 inhibitory potencies of amiodarone, dronedarone and their metabolites (Hong *et al.*, 2015; Karkhanis *et al.*, 2016). In this study, we observed a significantly slower rate of rivaroxaban clearance by CYP3A4 as compared to CYP2J2 during initial assay optimization (data not published). Our optimization culminated in two incubation time periods of 2 h and 30 min for the sensitive detection of inhibitory effects against CYP3A4 and CYP2J2 respectively.

We report for the first time the competitive inhibition as well as MBI of CYP3A4 and CYP2J2 by dronedarone and NDBD with rivaroxaban as the probe substrate. On the other hand, amiodarone and NDEA demonstrated mixed competitive inhibition of CYP3A4 but not CYP2J2. Similarly, MBI was established for amiodarone and NDEA with respect to CYP3A4 but not CYP2J2. Based on our reported K_i values (**Table 2**), both amiodarone and NDEA exhibited similar potencies for mixed competitive inhibition against CYP3A4 whereas dronedarone is a relatively more potent inhibitor of both CYP3A4 and CYP2J2 as compared to NDBD. For MBI, our results confirmed that the inactivation efficiency of NDEA was approximately threefold higher than that of amiodarone against CYP3A4 (**Table 3**). Between dronedarone and NDBD, dronedarone exhibited a stronger inactivation efficiency against CYP3A4 compared to NDBD while both dronedarone and NDBD demonstrated comparable CYP2J2 inactivation efficiency (**Table 3**).

DMD # 73890

Using two concentrations of rivaroxaban as the test substrate, our monolayer efflux studies also illustrated the non-competitive allosteric inhibition of P-gp mediated rivaroxaban efflux by amiodarone. This finding corroborated previous *in silico* studies which also predicted amiodarone to inhibit P-gp by noncompetitive allosteric inhibition (Seelig and Landwojtowicz, 2000). Based on the structural similarities of NDEA to amiodarone, NDEA was assumed to follow a similar mode of P-gp inhibition. Intriguingly, although dronedarone was determined to be a competitive inhibitor of P-gp efflux, NDBD demonstrated a minimal inhibitory effect on P-gp ($IC_{50} = 76.3 \mu M$). This observation deviates from previous postulation that dronedarone and NDBD may have a potential *additive to synergistic effect* on P-gp inhibition as is the case with amiodarone and NDEA (US FDA, 2009b).

The systemic exposures of NDEA and NDBD are comparable to that of their parent compounds and regulatory guidance proposes that metabolites present at $\geq 25\%$ of AUC of the parent drug warrant further consideration with regards to their potential in precipitating *in vivo* DDIs (US FDA, 2012). Taken together, our results indeed underscore the potential contributions of NDEA and NDBA as inhibitory metabolites. NDEA (k_{inact}/K_I : $387 \text{ min}^{-1}/\text{mM}^{-1}$) being a more potent time-dependent inactivator of CYP3A4 compared to amiodarone (k_{inact}/K_I : $130 \text{ min}^{-1}/\text{mM}^{-1}$) was consistent with previous *in vitro* studies using midazolam as a probe substrate (McDonald *et al.*, 2015). Likewise, NDEA (K_I : $5.36 \mu M$) being more potent than amiodarone (K_I : $8.94 \mu M$) in the inhibition of P-gp mediated rivaroxaban transport was also well aligned with previous transport assays using digoxin as a probe substrate (Katoh *et al.*, 2001). In summary, it is evident that a holistic prediction of *in vivo* clinical DDI would require consideration of the combined inhibitory effects of both the parent compound and its metabolite.

Comparison of inactivation parameters obtained in our study with previous in house data generated using US FDA validated probe substrates established a probe substrate differential response (**Supplemental Table 3**). In the case of CYP3A4, the inactivation efficiency (k_{inact}/K_I) of dronedarone and NDBD was greater when rivaroxaban was used as the probe substrate (i.e. 185 and $53.7 \text{ min}^{-1}/\text{mM}^{-1}$) as compared to testosterone (i.e. 44.8 and $15.9 \text{ min}^{-1}/\text{mM}^{-1}$). This phenomenon of probe

DMD # 73890

substrate-dependent inhibition profiles has been emphasized mainly for CYP3A4, which possesses multiple probe substrate binding regions within its active site (Kenworthy et al., 1999). Consequently, the interactions observed with one CYP3A4 probe may not accurately reflect those observed with another probe substrate (Galetin et al., 2005; Foti et al., 2010). Although CYP2J2 metabolism is generally restricted to a single active site, our findings suggested differential binding and metabolism among different substrates. Previous studies utilizing US FDA recommended astemizole demonstrated both reversible and irreversible inhibition of CYP2J2 metabolism by amiodarone (Lee *et al.*, 2012). However, our investigation revealed that amiodarone did not inhibit CYP2J2 reversibly and irreversibly with rivaroxaban as the probe substrate (**Supplemental Figures 3A-B**), suggesting the possibility of independent access of the active site of CYP2J2 by amiodarone and rivaroxaban (Shou *et al.*, 1994).

Taken together, our study (1) reiterates that the variability of *in vitro* inhibitory potencies against CYP3A4 and CYP2J2 is highly dependent on the choice of probe substrates and (2) confirms the importance of using specific victim drug as the probe substrate in enzyme and transporter interaction studies.

In our study, the static prediction of DDI between amiodarone, dronedarone and rivaroxaban yielded an AUC fold change of 1.22 and 1.17 respectively when inhibition of hepatic metabolism was considered (**Table 4**). Based on US FDA's guidelines (**Table 5**) (US FDA, 2012), this would imply that no significant inhibition was present. However, upon inclusion of gut metabolism, amiodarone and dronedarone were predicted to precipitate an AUC fold change in rivaroxaban exposure by 1.37 and 1.31 respectively. This attests to the significance of intestinal wall metabolism (Galetin *et al.*, 2007) which when ignored can under-estimate the extent of DDIs involving CYP3A4. Additionally, our results underscore the potential contribution of NDEA and NDBD to the eventual DDI magnitude, where AUC fold changes of 1.22 and 1.26 were observed respectively. Furthermore, the inhibition of P-gp mediated rivaroxaban efflux by amiodarone, NDEA and dronedarone was also predicted to independently produce AUC ratio increases of 1.09, 1.13 and 1.09 respectively. However, the

DMD # 73890

simultaneous influences of both parent drug and metabolite as well as the cumulative impact of enzyme-transporter interplay cannot be incorporated in the current static modeling. Moreover, there is also no consensus on an appropriate surrogate concentration of the inactivator/inhibitor $[I]_{in vivo}$ available to the enzyme. Typically, measures of $[I]_{in vivo}$ are selected based on the estimates that provide the best correlation between predicted and observed DDIs reported in literature (Fahmi *et al.*, 2008). Yet, in our case, our model cannot be cross-validated since clinical interaction data between rivaroxaban and amiodarone or dronedarone is not available. Nevertheless, it has been shown that model predictability was optimal when free portal steady state C_{max} was used for the reversible inhibition portion of the expression (term B) and free systemic steady state C_{max} was used for the time-dependent inactivation portion (term A) (Fahmi *et al.*, 2009). Hence, these validated estimates of $[I]_{in vivo}$ were adopted in our study to enhance DDI predictability.

Given that the *in vitro* interactions might culminate in a more significant DDI than that estimated using mechanistic static modeling, the use of PBPK models present several theoretical advantages. First, PBPK modeling utilizes a dynamic approach that allows consideration of changes in concentrations of enzyme, substrate and inactivator/inhibitor with time instead of relying on static point estimates. Second, PBPK modeling allows the evaluation of both intrinsic (e.g., organ dysfunction, age, genetics) and extrinsic (e.g., drug–drug interactions) factors, alone or in combinations, on drug exposure. Third, DDIs across multiple pathways and the variability of these DDIs in different populations can be examined.

Another factor that could potentially affect the *in vitro* to *in vivo* correlation is the presence of non-specific protein binding. The K_i , K_I and k_{inact} values were computed without accounting for protein binding in the recombinant system. Yet, Ishigam *et al.* has reported how the conversion of inhibition constants to their unbound values could eventually lead to more accurate predictions of the AUC-fold change upon co-administration of drugs (Ishigam *et al.*, 2001). Furthermore, considering the high protein binding of amiodarone, dronedarone and their metabolites, the derived *in vitro* inhibition and inactivation parameters might be relatively higher when unbound concentrations are considered.

DMD # 73890

Hence, to increase confidence in the DDI prediction, the fraction unbound in each incubation should be determined either computationally (Austin *et al.*, 2002) or through equilibrium dialysis experiments (Banker *et al.*, 2003).

In conclusion, amiodarone, dronedarone, NDEA and NDBD cause reversible inhibition and irreversible MBI of CYP3A4 with rivaroxaban as the probe substrate. Amiodarone and NDEA, unlike dronedarone and NDBD, do not inhibit CYP2J2. Amiodarone, dronedarone and NDEA but not NDBD, inhibit P-gp mediated efflux of rivaroxaban. Static modeling predicted a weak DDI risk between rivaroxaban and amiodarone or dronedarone. Fundamental limitations of the static model implied that molecular interactions between rivaroxaban and the antiarrhythmic agents and their metabolites via CYP3A4, CYP2J2 and P-gp were not considered in entirety. Future work would involve the assimilation of these *in vitro* inhibition parameters into a dynamic PBPK model, from which a more accurate quantitation of DDI magnitude can be derived.

DMD # 73890

AUTHORSHIP CONTRIBUTIONS

<i>Participated in research design:</i>	Cheong, Goh, Hong, Kojodjojo and Chan
<i>Conducted experiments:</i>	Cheong, Goh, Hong, Venkatesan and Liu
<i>Contributed new reagents or analytic tools:</i>	Chiu
<i>Performed data analysis:</i>	Cheong, Goh, Hong and Chan
<i>Wrote or contributed to the writing of the manuscript:</i>	Cheong, Goh, Hong and Chan

DMD # 73890

References

- Austin RP, Barton P, Cockcroft SL, Wenlock MC, and Riley RJ (2002) The influence of nonspecific microsomal binding on apparent intrinsic clearance, and its prediction from physicochemical properties. *Drug Metab Dispos* **30**:1497–503.
- Banker MJ, Clark TH, and Williams JA (2003) Development and validation of a 96-well equilibrium dialysis apparatus for measuring plasma protein binding. *J Pharm Sci* **92**:967–74.
- Chugh SS, Havmoeller R, Narayanan K, Singh D, Rienstra M, Benjamin EJ, Gillum RF, Kim YH, McAnulty JH, Zheng ZJ, Forouzanfar MH, Naghavi M, Mensah GA, Ezzati M, and Murray CJL (2014) Worldwide epidemiology of atrial fibrillation: A global burden of disease 2010 study. *Circulation* **129**:837–847.
- Fabre G, Julian B, Saint-Aubert B, Joyeux H, and Berger Y (1993) Evidence for CYP3A-mediated N-deethylation of amiodarone in human liver microsomal fractions. *Drug Metab Dispos* **21**:978–985.
- Fahmi OA, Hurst S, Plowchalk D, Cook J, Guo F, Youdim K, Dickins M, Phipps A, Darekar A, Hyland R, and Obach RS (2009) Comparison of different algorithms for predicting clinical drug-drug interactions, based on the use of CYP3A4 in vitro data: predictions of compounds as precipitants of interaction. *Drug Metab Dispos* **37**:1658–66.
- Fahmi OA, Maurer TS, Kish M, Cardenas E, Boldt S, and Nettleton D (2008) A combined model for predicting CYP3A4 clinical net drug-drug interaction based on CYP3A4 inhibition, inactivation, and induction determined in vitro. *Drug Metab Dispos* **36**:1698–708.
- Feng B, Hurst S, Lu Y, Varma M V., Rotter CJ, El-Kattan A, Lockwood P, and Corrigan B (2013) Quantitative Prediction of Renal Transporter-Mediated Clinical Drug–Drug Interactions. *Mol Pharm* **10**:4207–4215.
- Galetin A, Hinton LK, Burt H, Obach RS, and Houston JB (2007) Maximal inhibition of intestinal first-pass metabolism as a pragmatic indicator of intestinal contribution to the drug-drug interactions for CYP3A4 cleared drugs. *Curr Drug Metab* **8**:685–93.
- Gnoth MJ, Buetehorn U, Muenster U, Schwarz T, and Sandmann S (2011) In vitro and in vivo P-glycoprotein transport characteristics of rivaroxaban. *J Pharmacol Exp Ther* **338**:372–380.

DMD # 73890

- Grillo JA, Zhao P, Bullock J, Booth BP, Lu M, Robie-Suh K, Berglund EG, Pang KS, Rahman A, Zhang L, Lesko LJ, and Huang S-M (2012) Utility of a physiologically-based pharmacokinetic (PBPK) modeling approach to quantitatively predict a complex drug-drug-disease interaction scenario for rivaroxaban during the drug review process: implications for clinical practice. *Biopharm Drug Dispos* **33**:99–110.
- Hong Y, Chia YMF, Yeo RH, Venkatesan G, Koh SK, Chai CLL, Zhou L, Kojodjojo P, and Chan ECY (2015) Inactivation of Human Cytochrome P450 3A4 and 3A5 by Dronedarone and N-Desbutyl Dronedarone. *Mol Pharmacol* **89**:1–13.
- Ishigam M, Uchiyama M, Kondo T, Iwabuchi H, Inoue S, Takasaki W, Ikeda T, Komai T, Ito K, and Sugiyama Y (2001) Inhibition of in vitro metabolism of simvastatin by itraconazole in humans and prediction of in vivo drug-drug interactions. *Pharm Res* **18**:622–31.
- Isoherranen N, Lutz JD, Chung SP, Hachad H, Levy RH, and Ragueneau-Majlessi I (2012) Importance of multi-p450 inhibition in drug-drug interactions: evaluation of incidence, inhibition magnitude, and prediction from in vitro data. *Chem Res Toxicol* **25**:2285–300.
- January CT, Wann LS, Alpert JS, Calkins H, Cigarroa JE, Conti JB, Ellinor PT, Ezekowitz MD, Field ME, Murray KT, Sacco RL, Stevenson WG, Tchou PJ, Tracy CM, Yancy CW, Members F, Anderson JL, Halperin JL, Albert NM, Bozkurt B, Brindis RG, Creager MA, Curtis LH, Demets D, Guyton RA, Hochman JS, Kovacs RJ, Ohman EM, Pressler SJ, Sellke FW, Shen W-K, Stevenson WG, and Yancy CW (2014) 2014 AHA/ACC/HRS Guideline for the Management of Patients With Atrial Fibrillation.
- Karkhanis A, Lam HY, Venkatesan G, Koh SK, Chai CLL, Zhou L, Hong Y, Kojodjojo P, and Chan ECY (2016) Multiple modes of inhibition of human cytochrome P450 2J2 by dronedarone, amiodarone and their active metabolites. *Biochem Pharmacol* **107**:67–80.
- Kato M, Nakajima M, Yamazaki H, and Yokoi T (2001) Inhibitory effects of CYP3A4 substrates and their metabolites on P-glycoprotein-mediated transport. *Eur J Pharm Sci* **12**:505–513.
- Klieber S, Arabeyre-Fabre C, Moliner P, Marti E, Mandray M, Ngo R, Ollier C, Brun P, and Fabre G (2014) Identification of metabolic pathways and enzyme systems involved in the in vitro human hepatic metabolism of dronedarone, a potent new oral antiarrhythmic drug. *Pharmacol Res*

DMD # 73890

Perspect **2**:e00044.

Lee CA, Jones JP, Katayama J, Kaspera R, Jiang Y, Freiwald S, Smith E, Walker GS, and Totah RA (2012) Identifying a selective substrate and inhibitor pair for the evaluation of CYP2J2 activity.

Drug Metab Dispos **40**:943–51.

Lee CA, Neul D, Clouser-roche A, Dalvie D, Wester MR, Jiang Y, Iii JPJ, Freiwald S, Zientek M, Totah RA, Laboratories DJ, Diego S, California C a L, and Al LEEET (2010) Identification of Novel Substrates for Human Cytochrome. *Pharmacology* **38**:347–356.

McDonald MG, Au NT, and Rettie AE (2015) P450-Based Drug-Drug Interactions of Amiodarone and its Metabolites: Diversity of Inhibitory Mechanisms. *Drug Metab Dispos* **43**:1661–9.

Mueck W, Stampfuss J, Kubitza D, and Becka M (2014) Clinical pharmacokinetic and pharmacodynamic profile of rivaroxaban. *Clin Pharmacokinet* **53**:1–16.

Ohyama K, Nakajima M, Suzuki M, Shimada N, Yamazaki H, and Yokoi T (2001) Inhibitory effects of amiodarone and its N-deethylated metabolite on human cytochrome P450 activities: Prediction of in vivo drug interactions. *Br J Clin Pharmacol* **49**:244–253.

Orr STM, Ripp SL, Ballard TE, Henderson JL, Scott DO, Obach RS, Sun H, and Kalgutkar AS (2012) Mechanism-based inactivation (MBI) of cytochrome P450 enzymes: Structure-activity relationships and discovery strategies to mitigate drug-drug interaction risks. *J Med Chem* **55**:4896–4933.

Rahman F, Kwan GF, and Benjamin EJ (2014) Global epidemiology of atrial fibrillation. *Nat Rev Cardiol* **11**:639–654.

Seelig A, and Landwojtowicz E (2000) Structure-activity relationship of P-glycoprotein substrates and modifiers. *Eur J Pharm Sci* **12**:31–40.

Shou M, Grogan J, Mancewicz JA, Krausz KW, Gonzalez FJ, Gelboin H V, and Korzekwa KR (1994) Activation of CYP3A4: evidence for the simultaneous binding of two substrates in a cytochrome P450 active site. *Biochemistry* **33**:6450–5.

Steinberg BA, Hellkamp AS, Lokhnygina Y, Halperin JL, Breithardt G, Passman R, Hankey GJ, Patel MR, Becker RC, Singer DE, Hacke W, Berkowitz SD, Nessel CC, Mahaffey KW, Fox KAA, Califf RM, and Piccini JP (2014) Use and outcomes of antiarrhythmic therapy in patients with

DMD # 73890

atrial fibrillation receiving oral anticoagulation: Results from the ROCKET AF trial. *Hear Rhythm* **11**:925–932.

US FDA (2012) Guidance for Industry, Drug Interaction Studies — Study Design, Data Analysis, Implications for Dosing, and Labeling Recommendations.

US FDA (2009a) MULTAQ (dronedarone) briefing document.

US FDA (2009b) MULTAQ (dronedarone) clinical pharmacology and biopharmaceutics review.

US FDA (2011a) XARELTO (rivaroxaban). clinical pharmacology and biopharmaceutics review.

US FDA (2011b) XARELTO (rivaroxaban) product information.

Weinz C, Schwarz T, Kubitza D, Mueck W, and Lang D (2009) Metabolism and excretion of rivaroxaban, an oral, direct factor Xa inhibitor, in rats, dogs, and humans. *Drug Metab Dispos* **37**:1056–1064.

Yang J, Liao M, Shou M, Jamei M, Yeo KR, Tucker GT, and Rostami-Hodjegan A (2008) Cytochrome p450 turnover: regulation of synthesis and degradation, methods for determining rates, and implications for the prediction of drug interactions. *Curr Drug Metab* **9**:384–94.

Zhang L, Zhang YD, Zhao P, and Huang S-M (2009) Predicting drug-drug interactions: an FDA perspective. *AAPS J* **11**:300–306.

DMD # 73890

FOOTNOTES

This work was supported by the Singapore Ministry of Education Tier 1 Academic Research Funding [Grant R-148-000-193-112] and the National University of Singapore, Department of Pharmacy, Final Year Project Funding [Grant C-148-000-003-001] provided to Eric Chun Yong Chan.

Note: Eleanor Jing Yi Cheong, Janice Jia Ni Goh and Yanjun Hong contributed equally to the manuscript.

DMD # 73890

FIGURE LEGENDS

Figure 1. Chemical structures of (A) amiodarone, (B) dronedarone, (C) NDEA and (D) NDBD

Figure 2. Reversible inhibition of recombinant CYP2J2 (rCYP2J2) by dronedarone and NDBD. Formation rate of morpholinone hydroxylated metabolite was plotted against inhibitor concentration and fitted in the Michaelis–Menten kinetic model to calculate the inhibition constant K_i for (A) dronedarone and (B) NDBD towards rCYP2J2. Lineweaver–Burk plots (Fig. 2C-D) exhibit mixed competitive inhibition of rCYP2J2 by dronedarone and NDBD. Each point represents mean and S.D of triplicate experiments

Figure 3. Reversible inhibition of recombinant CYP3A4 (rCYP3A4) by amiodarone, NDEA, dronedarone and NDBD. Formation rate of morpholinone hydroxylated metabolite was plotted against inhibitor concentration and fitted in the Michaelis–Menten kinetic model to calculate the inhibition constant K_i for (A) amiodarone, (B) NDEA, (C) dronedarone and (D) NDBD towards rCYP3A4. Lineweaver–Burk plots (Fig. 3E-H) exhibit mixed competitive inhibition of rCYP3A4 by amiodarone and NDEA and competitive inhibition of rCYP3A4 by dronedarone and NDBD. Each point represents mean and S.D of triplicate experiments

Figure 4. Time- and concentration-dependent inactivation of recombinant CYP2J2 by (A) dronedarone and (B) NDBD using rivaroxaban as the probe substrate. Observed inactivation rates (k_{obs}) were plotted against inactivator concentrations to calculate the inactivation kinetic constants, k_{inact} and K_I for (C) dronedarone and (D) NDBD, respectively. Each point in (A and B) represents the mean and S.D. of triplicate experiments.

Figure 5. Time- and concentration-dependent inactivation of recombinant CYP3A4 by (A) amiodarone, (B) NDEA, (C) dronedarone and (D) NDBD using rivaroxaban as the probe substrate. Observed inactivation rates (k_{obs}) were plotted against inactivator concentrations to calculate the

DMD # 73890

inactivation kinetic constants, k_{inact} and K_I for (E) amiodarone, (F) NDEA (G) dronedarone and (H) NDBD, respectively. Each point in (A-D) represents the mean and S.D. of triplicate experiments.

Figure 6. Inhibition of P-gp mediated transport of 10 μM of rivaroxaban by amiodarone, NDEA, dronedarone and NDBD. IC_{50} values, determined by nonlinear regression, are (A) 10.3 μM for amiodarone, (B) 9.20 μM for NDEA, (C) 1.83 μM for dronedarone and (D) 76.3 μM for NDBD. Each point (in A-D) represents the mean and S.D. of triplicate experiments.

DMD # 73890

Table 1. Relevant *in vivo* concentrations of amiodarone, dronedarone and their metabolites that were incorporated into mechanistic static models

	Amiodarone	NDEA	Dronedarone	NDBD
$[I]_{\text{H (inactivation)}}^a$ (μM)	0.12	0.18	0.00063	0.0045
$[I]_{\text{H (reversible inhibition)}}^b$ (μM)	0.15	0.18 ^e	0.021	0.0045 ^e
$[I]_{\text{G}}^c$ (μM)	7.50	NA	40.4	NA
$[I]^d$ (μM)	2.99	2.80	0.21	0.21

^a $[I]_{\text{H (inactivation)}}$, concentration of inactivator at the enzyme active site in the liver defined as the systemic steady state unbound peak plasma concentration ($f_{u,b} \times C_{ss,max}$)

^b $[I]_{\text{H (inhibition)}}$, concentration of inhibitor at the enzyme active site in the liver defined as the hepatic portal inlet steady state unbound C_{max} ($f_{u,b} \times (\frac{D \times k_a \times F_a}{Q_H} + C_{ss,max})$) where D is total daily oral dose of the inhibitor, k_a is the oral absorption rate constant, F_a is the product of the fractions absorbed and escaping intestinal metabolism and Q_H is the hepatic blood flow (1450 mL/min)

^c $[I]_{\text{G}}$, concentration of inactivator/inhibitor at the enterocyte during absorption defined as $\frac{D \times k_a \times f_a}{Q_g}$ where f_a is the fraction of the inactivator/inhibitor dose absorbed into the gut wall and Q_g is the enterocytic blood flow (248 mL/min).

^d $[I]$: peak plasma concentration of the inhibitor

^e $[I]_{\text{H (reversible inhibition)}}$ for NDEA and NDBD is defined as the systemic steady state unbound peak plasma concentration

Drug-dependent parameters necessary for the derivations of these *in vivo* concentrations are presented in the **Supplementary Table 2.**

DMD # 73890

Table 2. CYP3A4 and CYP2J2 reversible inhibition kinetic parameters for amiodarone and NDEA, dronedarone and NDBD using rivaroxaban metabolite peak area ratio as a surrogate measurement of product formation. Data represented as mean \pm S.D.

CYP3A4	K_i (μM)
Amiodarone	0.226 ± 0.050
NDEA	0.239 ± 0.053
Dronedarone	0.64 ± 0.045
NDBD	1.03 ± 0.053
CYP2J2	K_i (μM)
Amiodarone	NA
NDEA	NA
Dronedarone	0.93 ± 0.11
NDBD	2.53 ± 0.33
NA not applicable	

DMD # 73890

Table 3. CYP3A4 and CYP2J2 inactivation kinetic parameters for amiodarone and NDEA, dronedarone and NDBD using morpholinone hydroxylation of rivaroxaban as a surrogate measurement of residual enzymatic activity. Data represented as mean \pm S.D.

CYP3A4	K_I (μM)	k_{inact} (min^{-1})	k_{inact}/K_I ($\text{min}^{-1}/\text{mM}^{-1}$)
Amiodarone	0.45 \pm 0.12	0.058 \pm 0.0045	129
NDEA	0.095 \pm 0.070	0.037 \pm 0.0056	389
Dronedarone	0.30 \pm 0.087	0.056 \pm 0.0046	185
NDBD	0.88 \pm 0.26	0.047 \pm 0.0052	53.7
CYP2J2	K_I (μM)	k_{inact} (min^{-1})	k_{inact}/K_I ($\text{min}^{-1}/\text{mM}^{-1}$)
Amiodarone	NA	NA	NA
NDEA	NA	NA	NA
Dronedarone	0.031 \pm 0.017	0.021 \pm 0.0017	677
NDBD	0.037 \pm 0.014	0.025 \pm 0.0014	676

NA not applicable

DMD # 73890

Table 4. Prediction of metabolic and transporter-mediated DDI upon concomitant administration of rivaroxaban with amiodarone, dronedarone and their metabolites using mechanistic static modeling

Precipitant	Predicted AUC Fold Change		
	Inhibition of hepatic metabolism	Inhibition of hepatic and gut metabolism	Inhibition of P-gp mediated efflux
Amiodarone	1.22	1.37	1.09
NDEA	1.22	NA	1.13
Dronedarone	1.17	1.31	1.09
NDBD	1.26	NA	n.d.

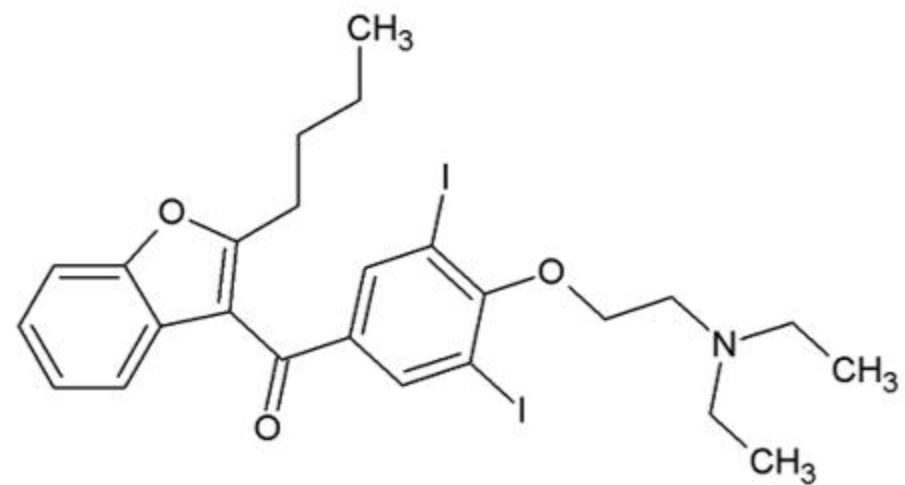
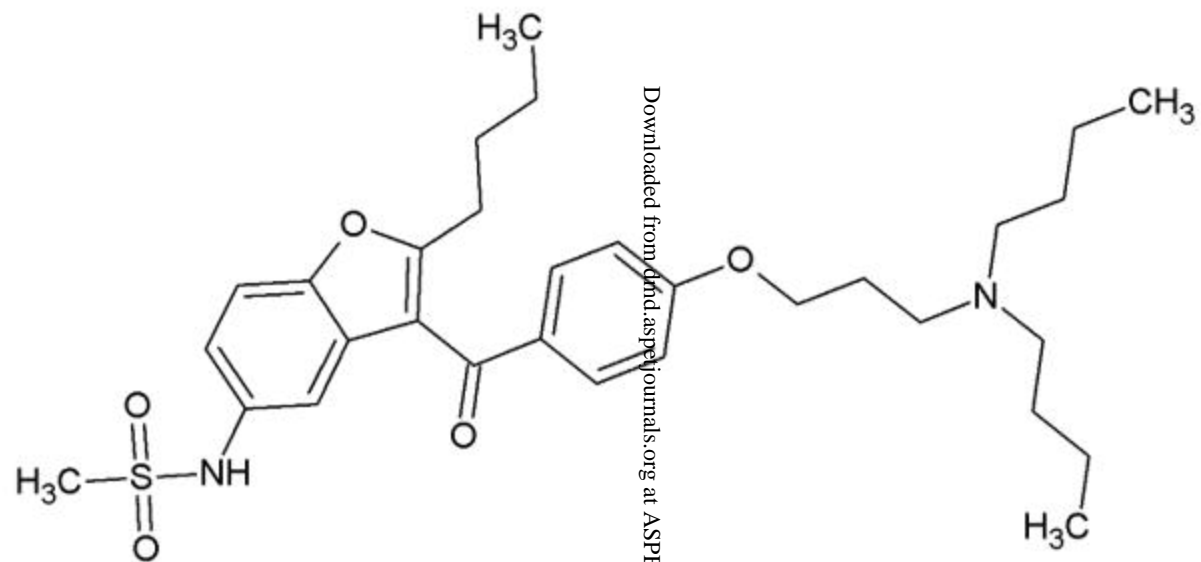
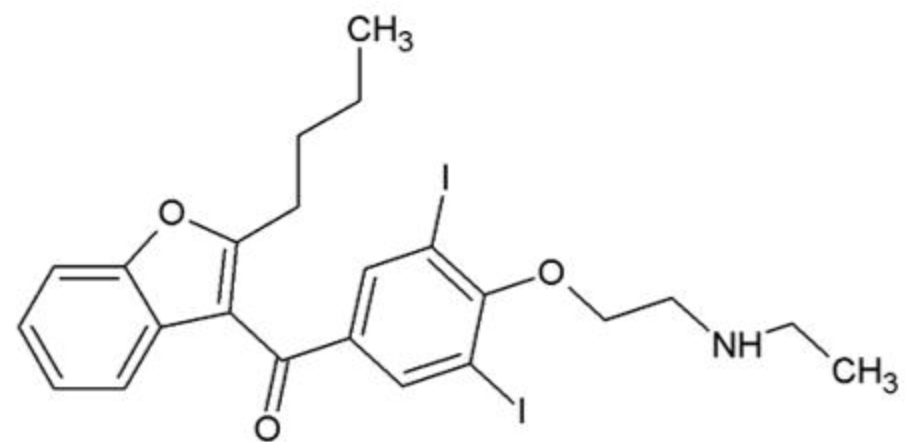
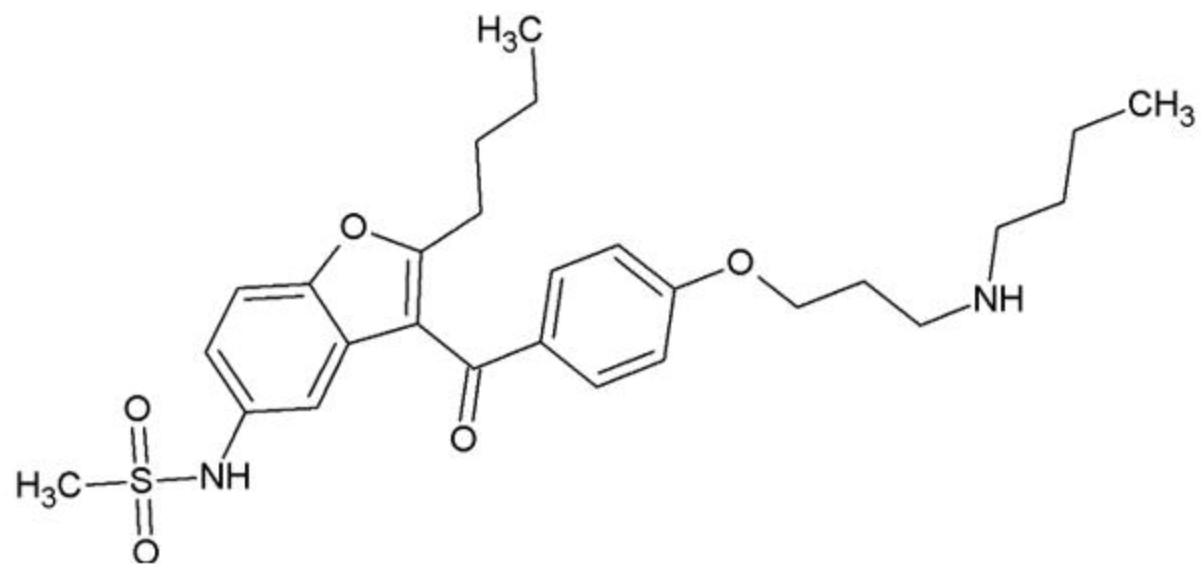
n.d. not determined

NA not applicable

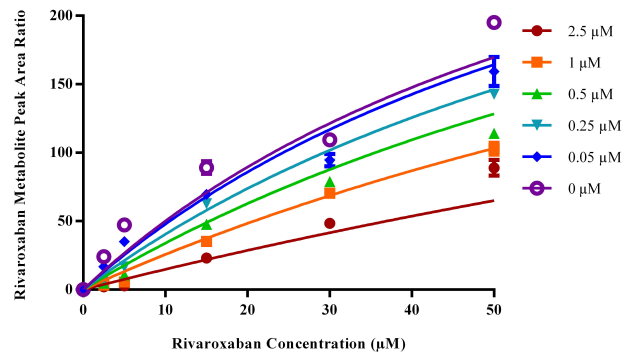
DMD # 73890

Table 5. US FDA Guidelines for Relative Risk of DDIs based on Observed Increases in AUC for
Victim Drug

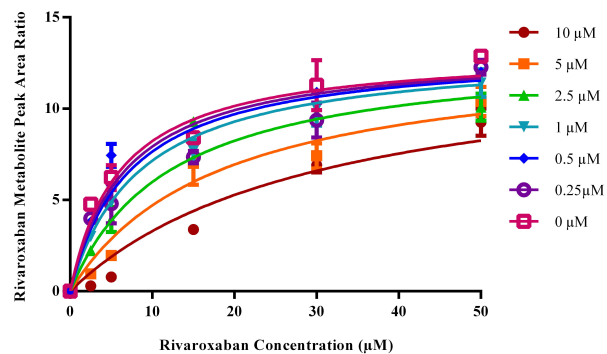
Category of Relative Risk	Observed Changes in AUC
Strong DDI	≥ 5 -fold increase in AUC
Moderate DDI	≥ 2 but < 5 -fold increase in AUC
Weak DDI	≥ 1.25 but < 2 -fold increase in AUC

A**B****C****D****Figure 1**

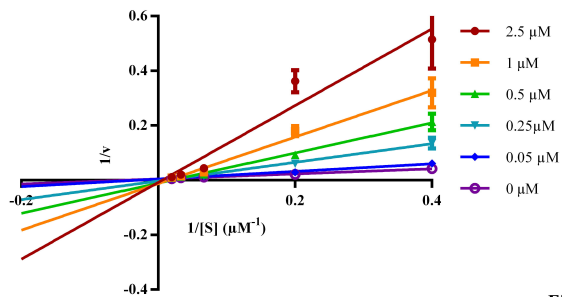
A



B



C



D

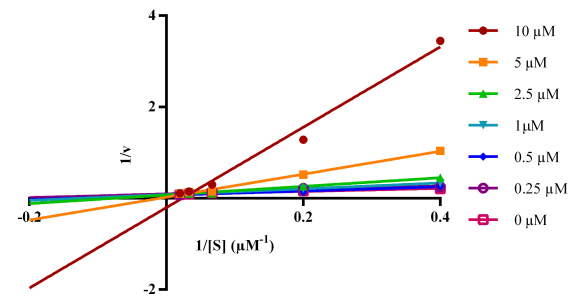
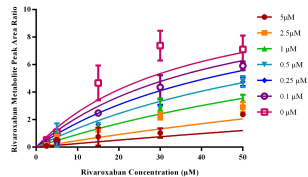
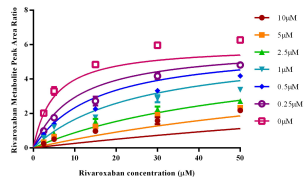


Figure 2

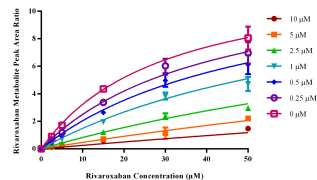
A



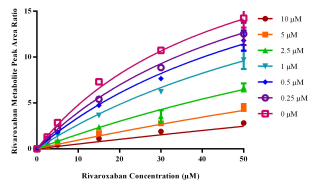
B



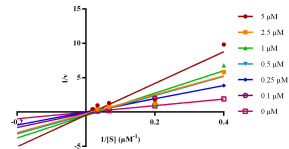
C



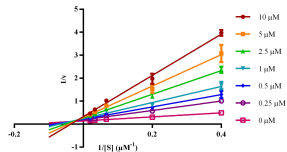
D



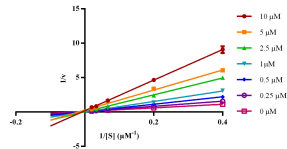
E



F



G



H

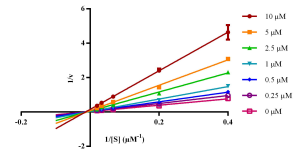
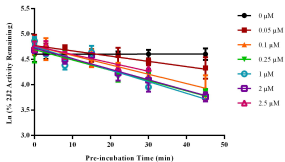
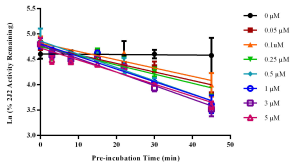


Figure 3

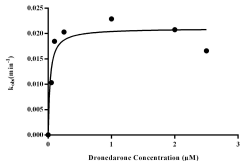
A



B



C



D

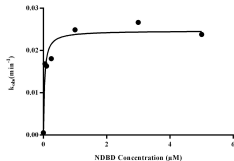
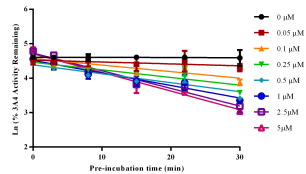
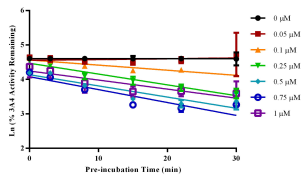


Figure 4

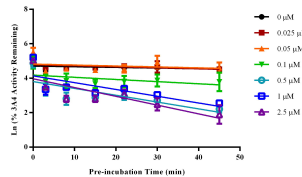
A



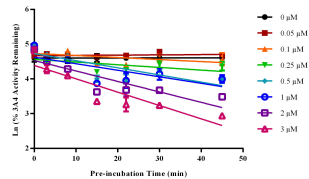
B



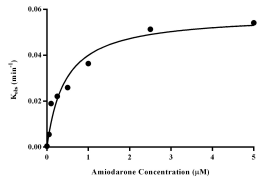
C



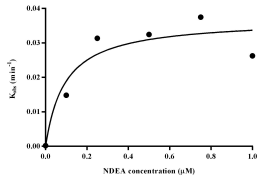
D



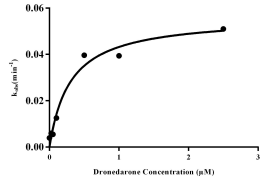
E



F



G



H

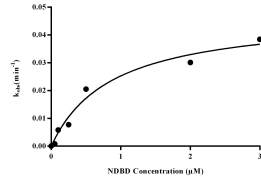
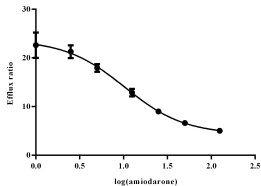
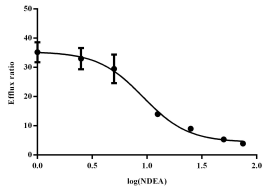


Figure 5

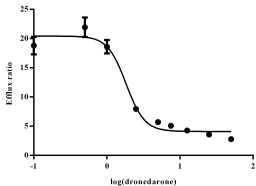
A



B



C



D

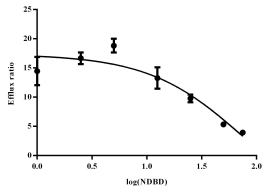


Figure 6